Heliyon 7 (2021) e06291

Contents lists available at ScienceDirect

Heliyon

journal homepage: www.cell.com/heliyon

Research article

The effect of pressure variation on droplet size distribution of dispersed oil under simulated deep-water conditions

Xing Song [a], Liang Jing [a,b], Bing Chen [a,*], Zhiwen Zhu [a], Qinhong Cai [a,c], Xudong Ye [a], Xiao Zheng [a], Stephen J. Hill [d], Baiyu Zhang [a]

[a] Northern Region Persistent Organic Pollution Control (NRPOP) Laboratory, Faculty of Engineering and Applied Science, Memorial University of Newfoundland, St. John's, NL A1B 3X5, Canada
[b] Department of Chemical and Petroleum Engineering, Schulich School of Engineering, University of Calgary, Calgary, AB T2N 1N4, Canada
[c] Department of Natural Resource Sciences, McGill University, Anne de Bellevue, QC H9X 3V9, Canada
[d] Department of Ocean Sciences, Memorial University of Newfoundland, St. John's, NL A1B 5S7, Canada

ARTICLE INFO

Keywords:
Marine oil spill
Chemically dispersed oil
Droplet size distribution
Deep-water
High pressure
Mixing energy

ABSTRACT

Droplet size distribution of dispersed oil in deep-water is critical to the transport and biodegradation of spilled oil in deep-sea. Few studies have focused on the effects of pressure on chemically dispersed oil through experiments. This study thus simulated how the crude oil homogenously pre-dispersed by Corexit 9500A using baffled flasks would behave after being exposed to deep-water conditions. Key factors included dispersant-to-oil ratio (DOR), mixing energy (energy dissipation rate and Kolmogorov microscale), and pressure (up to 150 bar). The variations of pressure were demonstrated to have insignificant effects on the size distribution of pre-dispersed oil. Both the average and medium droplet sizes were correlated negatively with DOR and mixing energy in an established model with a p-value ≤ 0.0011. The log-normal and log-logistic distributions provided a reasonable fit to simulate the droplet size distribution. The two parameters of log-logistic distribution were dependent on DOR and mixing energy with a p-value < 0.005. The results would be valuable to advance the understanding of the behaviours and trajectories of chemically dispersed oil under deep-water conditions. The research helped provide more scientific evidence to improve the understanding of dispersed oil behaviours under high pressure and support deep-sea oil spill research and potential extension of the existing results from shallow water to deep water conditions.

1. Introduction

The Deep Water Horizon (DWH) oil spill happened in April 2010 led to a release of roughly 5 million barrels of crude oil and gas in the depth of around 1,500 m. This disaster was recorded as the largest accidental marine oil spill resulting in huge ecological impacts and an estimated total liability of 100 billion USD (Griggs, 2011; Turner et al., 2019). Over 2.1 million gallons of oil dispersant was applied at both the surface and wellhead in the Gulf Mexico to decrease the size of oil droplets and increase the oil fractions trapped in subsurface (Kujawinski et al., 2011; Spier et al., 2013). This is the first real application of large amounts of dispersant in deep-water conditions. Afterwards, many efforts began to focus on the fate and transport of spilled oil, especially the chemically dispersed oil, using DWH oil spill for modification and verification. An important consensus was that the relatively smaller oil droplets were prolonged trapped in water column while larger oil droplets could fast reach the surface of the ocean (Lindo-Atichati et al., 2016a; Ryerson et al., 2012). In comparison of oil droplet size, its distribution plays an even more essential role in determining the fate and transport of released oil in deep-water environment as well as the intrinsic mechanisms of oil dispersion (Gong et al., 2014; Li et al., 2011b; North et al., 2015; Zhao et al., 2014a). The sizes of dispersed oil highly affected the spatial distribution of oil in the ocean, resurfacing rate, and oil dissolution (North et al., 2015; Scheibye et al., 2017). Dispersed oil with smaller sizes were more readily degraded in submarine environment and deep-water conditions (Aman et al., 2015; North et al., 2015; Vilcáez et al., 2013). However, knowledge is still limited to better understand the behaviours of dispersed oil associated with the possible variations of droplet size in deep-water.

Many efforts have been undertaken to predict or simulate the formation of dispersed oil under various operating and thermodynamic conditions (Brandvik et al., 2013; Li et al., 2016; Malone et al., 2018;

* Corresponding author.
E-mail address: bchen@mun.ca (B. Chen).

https://doi.org/10.1016/j.heliyon.2021.e06291
Received 6 May 2020; Received in revised form 20 September 2020; Accepted 11 February 2021

Zhao et al., 2016a). Many operating conditions can lead to diverse patterns of droplet size distribution. For example, Brandvik et al. (2013) observed the fluctuation of oil droplet size distribution with the variation of oil spill operating parameters, containing nozzle diameters, oil flow rate, the addition of air, and addition of dispersants with different dispersant-to-oil ratio (DOR). Methane dissolved in oil dramatically increased the median size of oil droplets (Malone et al., 2018). Thermodynamic factors mainly included pressure fluctuation caused by turbulence, resistance force due to interfacial tension and oil viscosity, pressure, temperature, and other related parameters such as oil droplet velocity and turbulent velocity of an eddy (Chen and Yapa, 2007; Johansen et al., 2013; Li et al., 2016; Zhao et al., 2017). Intrusions found in the DWH oil spill were driven by horizontal currents and stratification (Socolofsky et al., 2011). Chen and Yapa (2007) correlated thermodynamic parameters, such as oil droplet release velocity, the density of seawater and interfacial tension, into the estimation of maximum droplet size for the probability density function of droplet size distribution in deep-water. However, whether the pressure can significantly alter the droplet size and the structure of dispersed oil existing in deep-water was less tackled through experiments.

The variation of pressure may alter the behaviours of dispersed oil, though the impacts on the droplet sizes might be unapparent due to the low compressibility of liquids (Malone et al., 2018). In DHW spill site, the oil density at seafloor obtained based on empirical calculation was 4.5 % higher than the sea surface oil density by acoustic measurement (Camilli et al., 2011; Socolofsky et al., 2011). With the presence of dispersant, approximately 31% of interfacial tension between oil and water was enhanced because of increasing pressure, implying a less effective dispersion in deep-water conditions (Abdelrahim, 2012). The change of interfacial tension reflected the alternation of the destabilization of surfactants and the possible change of droplet size controlled by high pressure (Johansen et al., 2013; Khelifa and So, 2009). All these shreds of evidence suggested that higher pressure may affect the droplet properties of dispersed oil and the stability of the emulsion structure (Chen and Yapa, 2007). While whether these changes were statistically significant to the droplet size of dispersed oil under high pressure had not been reported leading to the need for scientific verification. More experimental observations were preferred to verify the model regarding oil droplet distribution (Gros et al., 2016; Johansen et al., 2013; Malone et al., 2018).

Meanwhile, dispersed oil could be widely distributed in the water column after an oil spill. In the oil plume (35 km long and 1100 m depth) after the BP oil spill, the methane levels were only discovered at 500 m horizontal distance from the center of the oil plume, the distribution of methane and other gas was approximately 0 % at the other parts of the oil plume (Camilli et al., 2010). Additionally, gas bubbles had been demonstrated easily separated from the water phase of the plume due to their buoyancy (Johansen, 2003; Socolofsky, 2001). Dispersed oil could be a non-negligible formation of oil plume in the water column at the deep sea. The research on dispersed oil was essential and valuable for understanding their behaviours and the effects of subsea dispersant injection.

The above-stated knowledge gap was filled in this study. The impact of pressure on the size distribution of chemically pre-dispersed oil (CDO) droplets was investigated after being exposed to deep-water under various dispersant-to-oil ratio (DOR) and mixing energy (i.e., shaking rate). The performance of CDO droplet size prediction was evaluated using statistical tools. The research outputs would help to understand and predict the fate of CDO under deep-water conditions to support contingency planning, emergency response, and decision making.

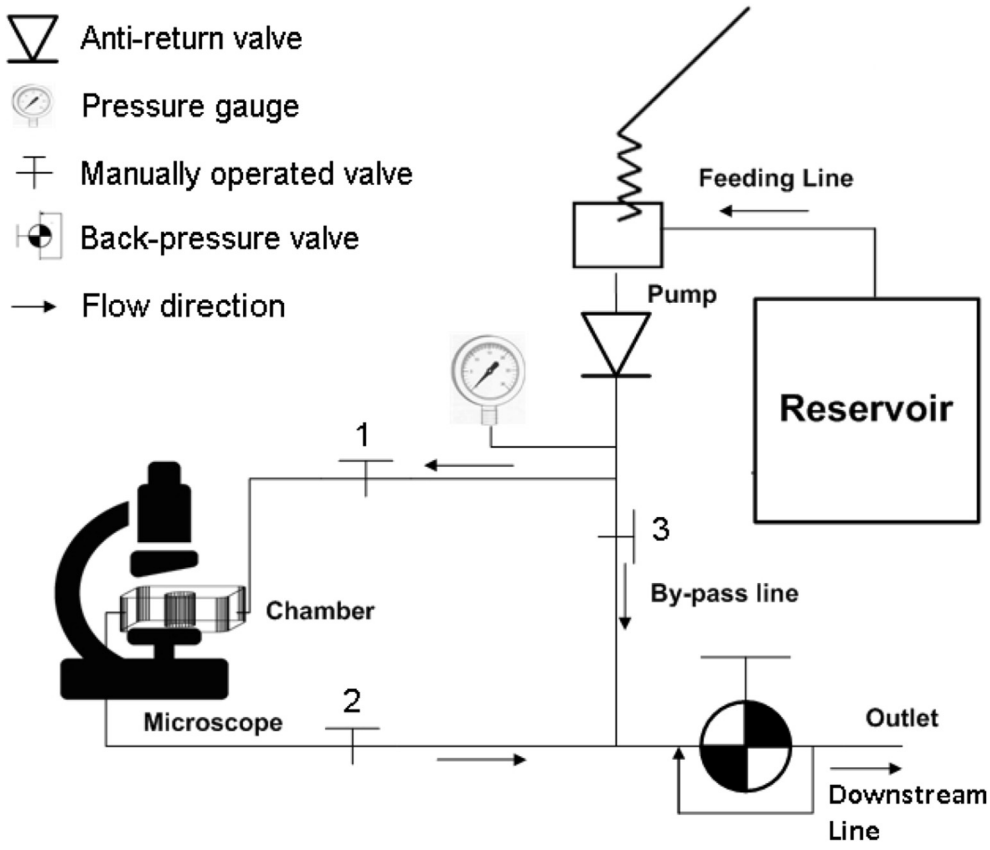

Figure 1. Schematic drawing of the high-pressure microscope system.

Table 1. Two-level factorial experimental design.

Factor	Levels	Unit	Values	
DOR	2	-	1:32.5	1:17.5
Mixing energy (Shaking rate)	2	m^2/s^3 (rpm)	$9.79*10^{-2}$ (160)	3.23 (240)
Pressure	2	bar	50	150

2. Methodology

2.1. Materials and chemicals

Experiments were conducted using Alaska North Slope (ANS) crude oil (viscosity 50.1 cP at 21 °C, from Environment Canada) and Corexit 9500 (Nalco, Naperville, IL). Unpolluted seawater was obtained from 30 m water depth at Ocean Science Center, Memorial University in St. John's, Canada, and pre-filtered to remove unwanted organisms and particles.

2.2. The high-pressure microscope system

As shown in Figure 1, the high-pressure microscope system contains a plumbing system, a sealable PRISM (PICCEL Related Imaging System for Microscopy) chamber (Pradillon et al., 2004), and a light microscope. A similar high-pressure system was successfully applied to determine the biodegradation of the GC-detectable hydrocarbons (Prince et al., 2016). The plumbing system has a liquid reservoir where seawater, RO water, or ethanol can be stored. There are five valves used in the plumbing system, including an anti-return valve, a back-pressure valve, a by-pass valve, and two manually operated valves to control the inlet and outlet of the PRISM chamber. The feeding line is used to provide the desired liquid to the system, whereas the downstream line is designed to set and control the working pressure by setting the back-pressure valve. All pipes and valves are made of stainless steel. A single-acting, single-piston air-driven hand-pump (ACHL189-01, Parker Corporate, USA) is used to continuously pump the liquid (max 0.25 L/min at 300 bar maximum outlet pressure) from the reservoir through the feedline line and pressurize it when the back-pressure valve is engaged.

The PRISM chamber includes a stainless-steel body (50 × 40 × 20 mm) with two lateral openings. A threaded observation column (7 mm in diameter and 5 mm in height) is available at the center where a 3 mm thick sapphire window is mounted by a Viton seal, a Teflon washer, and a hollow steel screw at the top and bottom, respectively. The valid working volume is approximate 0.2 ml when the column is sealed with windows. The chamber is connected to the plumbing system through valves 1 and 2 such that pressure is controlled by closing valve 3 and adjusting the back-pressure valve. The pressure can be held by the anti-return valve for at least 24 h. The observation of droplet size was done with a Nikon SMZ745 microscope equipped with an Infiniti1 2.0-megapixel CMOS microscopy camera (Infinity, USA) focusing on the window of the chamber. The images captured by the camera are 1600 × 1200 pixels and encompassed an area of 6.72 × 5.04 mm. Therefore, the length of each pixel is approximately 4.2 μm.

2.3. Experimental design

A two-level factorial design (Table 1) was employed to determine the impacts of pressure associated with DOR and mixing energy on the droplet sizes of dispersed oil as well as their possible interactions using Design-Expert® software (Design-Expert® version 8.0.5b; State-Ease Inc., Minneapolis, MN, USA). The shaking rate, an important factor correlated to turbulence kinetic energy, was set as 160 and 240 rpm, given the dispersion performance at 150 rpm was significantly reduced, and the number of countable droplets was relatively small. DOR was tested at 1:32.5 and 1:17.5. The pressure was chosen as 50 and 150 bar to account for deep-water (high pressure) conditions at water depth from 500 to 1500 m, respectively (Lemaire et al., 2012). The levels were determined based on preliminary experimental runs and recommendations from the literature (Kaku et al., 2006; Venosa et al., 2002). The average and median of oil droplet radii were selected as the responses. Overall, a design of eight experiments was conducted in a random order to minimize the impact of confounding factors. Seawater temperature was maintained at 10 °C during the tests.

To explore the possible effects of pressure loss on the droplet size distribution, a preliminary experiment was performed with multiple conditions at 200 rpm (mixing energy 0.563 m^2/s^3). DOR was tested at 1:25. The pressure was decreased from 150 bar to 0 bar in 10 min. The variances of oil droplet radii were observed and recorded.

2.4. Experimental procedure

For each of the experimental runs, 120 ml pre-filtered seawater was added into a baffled flask, followed by adding 100 μL crude oil onto the water surface using a repeater pipette (Venosa and Holder, 2007; Venosa et al., 2002; Zhang et al., 2018). Then Corexit 9500A was added onto the center of the oil slick according to the preset oil-to-dispersant ratio. The flask was placed on the orbital shaker and vigorously mixed for 10 min at the preset shaking rate to provide mixing energy for dispersion. At the end of the mixing procedure, the flask was removed from the shaker, and stand for another 10 min. Non-dispersed oil could rise to the surface of the seawater. The stopcock at the bottom of the flask was opened to drain the first 2 ml of the sample before collecting another 5 ml oil-water mixture sample for observation.

The microscope system was thoroughly washed with RO water and ethanol prior to and after each use. The PRISM chamber was refilled with seawater (valves 1 and 2 open, and valve 3 closed) from the reservoir until water dropped from the back-pressure valve at normal pressure. Seawater was then removed from the inside of the chamber when value 2 was turned off. The clean chamber as then filled with chemically dispersed oil. The chamber was successfully sealed only when few bubbles could be observed through the microscope. The pump was actuated continuously to increase the pressure to the preset level while the sample was maintained in the chamber. It was assumed that the amount of seawater injected into the chamber was negligible. The pressure was maintained for 5 min prior to capturing pictures in order to stabilize the sample for imaging. Based on the homogeneity assumption, images were captured at the top focal layer (lens) and four other layers that were randomly selected between the top and bottom of the PRISM chamber.

Image processing was carried out using ImageJ software (National Institutes of Health, USA), and the radius of each droplet was manually measured and recorded in μm units. For each image, around 400 and 100 droplets were randomly selected from the images captured at the top layer and the other four layers, respectively, for a total of around 800 droplets. van der Tuuk Opedal et al. (2009) suggested that at least 800 droplets are required to obtain a credible impression of oil droplet size.

2.5. Calculation of mixing energy based on the shaking rate

The velocity fields (average radial and azimuthal velocities) were measured at different levels of shaking rates (100–250 rpm) in baffled flasks test system (Kaku et al., 2006; Zhao et al., 2016b). The shaking rate associated with the water velocity had a linear relationship with mixing energy, involving energy dissipation rate and Kolmogorov microscale at

the range from 100-250 rpm. The mixing energy can be estimated through Eqs. (1) and (2):

$$\overline{\varepsilon} = 9.0 \times 10^{-5} \times e^{0.0437\Omega} \quad (1)$$

$$\overline{\eta} = 1.463 \times 10^{3} \times e^{-0.015\Omega} \quad (2)$$

where $\overline{\varepsilon}$ was the average of energy dissipation rate, $\overline{\eta}$ denoted the average of Kolmogorov microscale, Ω was the shaking rate from 100 to 250 rpm. These energy-based parameters have been widely applied in the modeling and mechanisms exploration for the fate and behaviours of dispersed oil, especially the droplet size distribution (Dippner, 2009; Khelifa et al., 2002; Li and Garrett, 1998; Zhao et al., 2014b). Therefore, the range of the shaking rates (160–240) in this study is meaningful and transferable to the mixing energy in non-breaking and breaking wave conditions at sea.

2.6. Statistical analysis

All experimental data were subjected to analysis of variance (ANOVA) to determine the significance of DOR, shaking rate, and pressure on both responses (i.e., average and median radii). ANOVA tests the null hypothesis that the output means of each factor level are equal, versus them not being equal. A probability of $p < 0.05$ indicates that this factor or the interaction between multiple factors is significant.

Previous studies have simulated the distribution of oil droplet size (Aman et al., 2015; Brandvik et al., 2014; Johansen et al., 2013; Li et al., 2017). The form and shape of log-logistic distribution were close to those of lognormal and Rosin-Rammler distributions (Babinsky and Sojka, 2002). In this paper, log-normal and Log-logistic distribution regressions were applied to predict droplet size for each experimental run using Minitab 17.0. Log-logistic distribution could be described by the following Eq. (3):

$$f(x) = \frac{1}{b(x-\theta)} \frac{e^{-((log(x-e)-\alpha)/\beta)}}{\left[1 + e^{-((log(x-e)-\alpha)/\beta)}\right]^2},\ x > \theta,\ \beta > 0 \quad (3)$$

where α and β are the parameters related to the average value and the variation of the sample, respectively. They were also expressed as "loc" and "scale" in Figures.3 and 4, respectively. The values of α and β for each experimental run were further used as ANOVA responses to determine the effect of DOR, shaking rate, and pressure on the shape of distribution.

3. Result and discussion

3.1. ANOVA of droplet radius

The detectable droplet size of dispersed oil generated in normal pressure ranged from 8-200 μm with 50 μm of average and 44 μm of the medium. This range is compatible with the droplet size distribution in other studies though the conditions are different. For example, the droplet size of Louisiana Sweet crude oil under 150 bar was 16–200 μm with 57 μm of medium diameter (Malone et al., 2018). The simulated mean of oil droplet size without dispersants decreased from 344 to 125 μm with the increase of mixing energy (Aman et al., 2015).

The coded mathematical model for a 2^3 full factorial design can be given as:

$$R^{\lambda} = X_0 + X_1A + X_2B + X_3C + X_4AB + X_5AC + X_6BC + X_7ABC \quad (4)$$

where R is the average or medium droplet radius (μm); λ is the transformation parameter to improve the accuracy of the model (default at 1); X_0 represents the global mean droplet radius (μm); X_i ($i = 1$–7) represent the regression coefficients of the individual and synergetic effects of DOR, mixing energy, and pressure; and A, B, and C are coded input values of -1 or 1 to correspondingly represent the low and high levels of DOR, mixing energy, and pressure at 1:32.5 and 1:17.5, 0.0979 and 3.23 m^2/s^3 (132.7–39.97μm for Kolmogorov microscale), and 50 and 150 bar, respectively (Table 2). The Box–Cox (B–C) plots for power transforms suggested that a power transformation (λ = -1.81 for average and λ = -1.44 for median) of the original outputs would better normalize the data points. The average and median radii of CDO droplet under different experimental conditions can be expressed as the following equations:

$$Average^{-1.81} = 3.293 \times 10^{-3} + 4.935 \times 10^{-4}A + 8.494 \times 10^{-4}B \quad (5)$$

$$Median^{-1.44} = 0.012 + 1.198 \times 10^{-3}A + 1.510 \times 10^{-3}B \quad (6)$$

Eqs. (5) and (6) indicate that the decrease of A (i.e., DOR) and B (mixing energy) can result in a larger droplet radius. Results from ANOVA on the transformed and coded response models were summarized in Tables 3 and 4. From the Fisher's *F*-test, it was observed that the established models (Eq. (5) and (6)) were statistically significant with *F*-values of 123.34 and 35.89, respectively, and probability values ($Prob > F$) all less than 0.05. This observation was also verified by the high adjusted and predicted R^2 values, which indicated that the models could accurately predict the average and median droplet radii, respectively. The predicted R^2 values of 0.95 and 0.83 meant that 95 and 83% of the sample variation could be attributed to the independent variables. The adjusted R^2 values of 0.97 and 0.91 were close to the predicted R^2 and were also of statistical significance and agreed with the correlation applicability of both models.

According to Tables 3 and 4, a factor or an interaction with a *p*-value less than 0.05 is defined as having a significant influence on oil droplet size. The smaller the *p*-values are, the greater the significance of the factors or their interactions. It can be observed that the shaking rate was the most influential factor, followed by DOR. The effect of pressure and other interactions were not prominent. This finding agreed well with the fact that the coefficients of B, as shown in Eqs. (5) and (6), were greater than those of DOR.

As depicted in Figure 2 and Figure 3, the contour plots of ANOVA illustrate the correlations between each pair of factors. It was observed that the size of dispersed oil droplet grew (both average and median radii) with decreasing DOR and/or shaking rate (mixing energy) (Figures. 2 (a) and 3 (a)). However, the increase of median value (i.e., from 19 to 25 μm) was not as significant as that of average value (i.e., from 19 to 32 μm). This observation might imply that the number and size of droplets smaller than 19–25 μm remained unchanged, while the size of droplets larger than this seemed to be further enlarged. In addition, the influence of DOR at low mixing energy (25–32 μm for 0.0979 m^2/s^3) was more prominent than that at high mixing energy (19–22 μm for 3.23 m^2/s^3) as shown in Figure 2 (a), while the effect of shaking rate at high DOR (22–32 μm) was more noticeable than that at low DOR (19–25 μm). Figures.2 (b) and 3 (b) further indicated that altering pressure after dispersion did not contribute appreciably to any droplet size change.

3.2. Effect of pressure on oil droplet sizes under various DOR and mixing energy

The pictures of oil droplets were shown in Figure 4. The pressure did not show any statistically significant correlation with droplet size of CDO in this experiment. Preliminary experiments, when the pressure was changed from 0, 50, 150, and 200 bar with the same DOR (1:32.5) and mixing energy (0.562 m^2/s^3, 200 rpm), the radius of droplet size did not change significantly. This observation had a practical significance in the application of dispersants under deep-water environments. The insignificant effect implied that CDO droplets, once fully dispersed, may not have a remarkable variation in size. The result was an agreement with the negligible effect of the pressure on droplet size distribution of crude oil in Deepwater as well as the assumptions (Abdelrahim, 2012; Malone et al., 2018). The observed increase of droplet size in the experiments was the coalescence on the top of glass lens due to the resurfacing of droplets by

Table 2. Factorial design matrix of three factors with experimental responses for the average and median of droplet radius.

Std	Run	A: DOR	B: Mixing energy	C: Pressure	Response 1 Average (μm)	Response 2 Median (μm)	a	b
2	m	-1	-1	-1	33.25	25.08	3.257	0.2399
1	x	1	-1	-1	25.14	21.97	3.132	0.1867
4	y	-1	1	-1	21.95	21.19	3.060	0.1409
7	xyz	1	1	1	19.08	18.35	2.893	0.1302
5	xz	1	-1	1	25.12	21.97	3.143	0.1760
3	xy	1	1	-1	19.81	19.68	2.945	0.1187
8	yz	-1	1	1	22.62	21.19	3.058	0.1215
6	z	-1	-1	1	29.60	27.74	3.325	0.1903

Table 3. ANOVA for the transformed response of average droplet radius.

Source	Sum of squares	*df*	Mean square	*F*-value	*p*-value (Prob > *F*)	
Model	7.72×10^{-6}	2	3.86×10^{-6}	123.34	<0.0001	significant
A	1.95×10^{-6}	1	1.95×10^{-6}	62.25	0.0005	
B	5.77×10^{-6}	1	5.77×10^{-6}	184.43	<0.0001	
Residual	1.57×10^{-7}	5	3.13×10^{-8}			
Total	7.88×10^{-6}	7				

Table 4. ANOVA for the transformed response of median droplet radius.

Source	Sum of squares	*df*	Mean square	*F*-value	*p*-value (Prob > *F*)	
Model	2.97×10^{-5}	2	1.49×10^{-5}	35.89	0.0011	significant
A	1.15×10^{-5}	1	1.15×10^{-5}	27.72	0.0033	
B	1.82×10^{-5}	1	1.82×10^{-5}	44.06	0.0012	
Residual	2.07×10^{-6}	5	4.14×10^{-7}			
Total	3.18×10^{-5}	7				

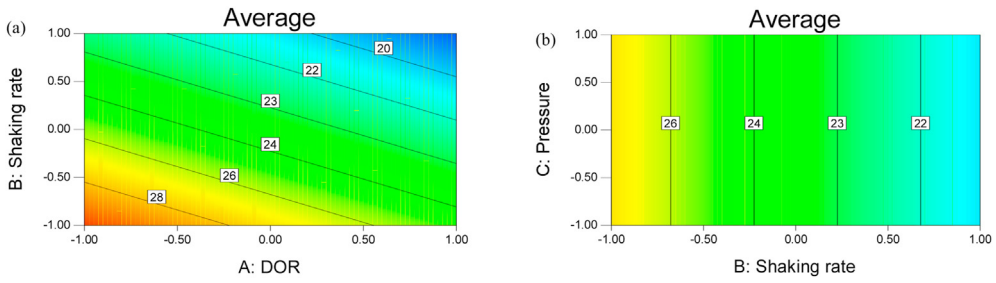

Figure 2. Influence on average droplet radius by factor interactions: (a) DOR and shaking rate (mixing energy), and (b) shaking rate (mixing energy) and pressure.

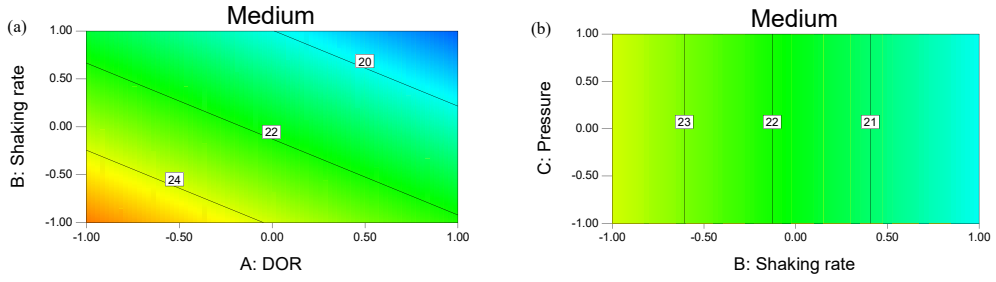

Figure 3. Influence on median droplet radius by factor interactions: (a) DOR and shaking rate (mixing energy), (b) shaking rate (mixing energy) and pressure.

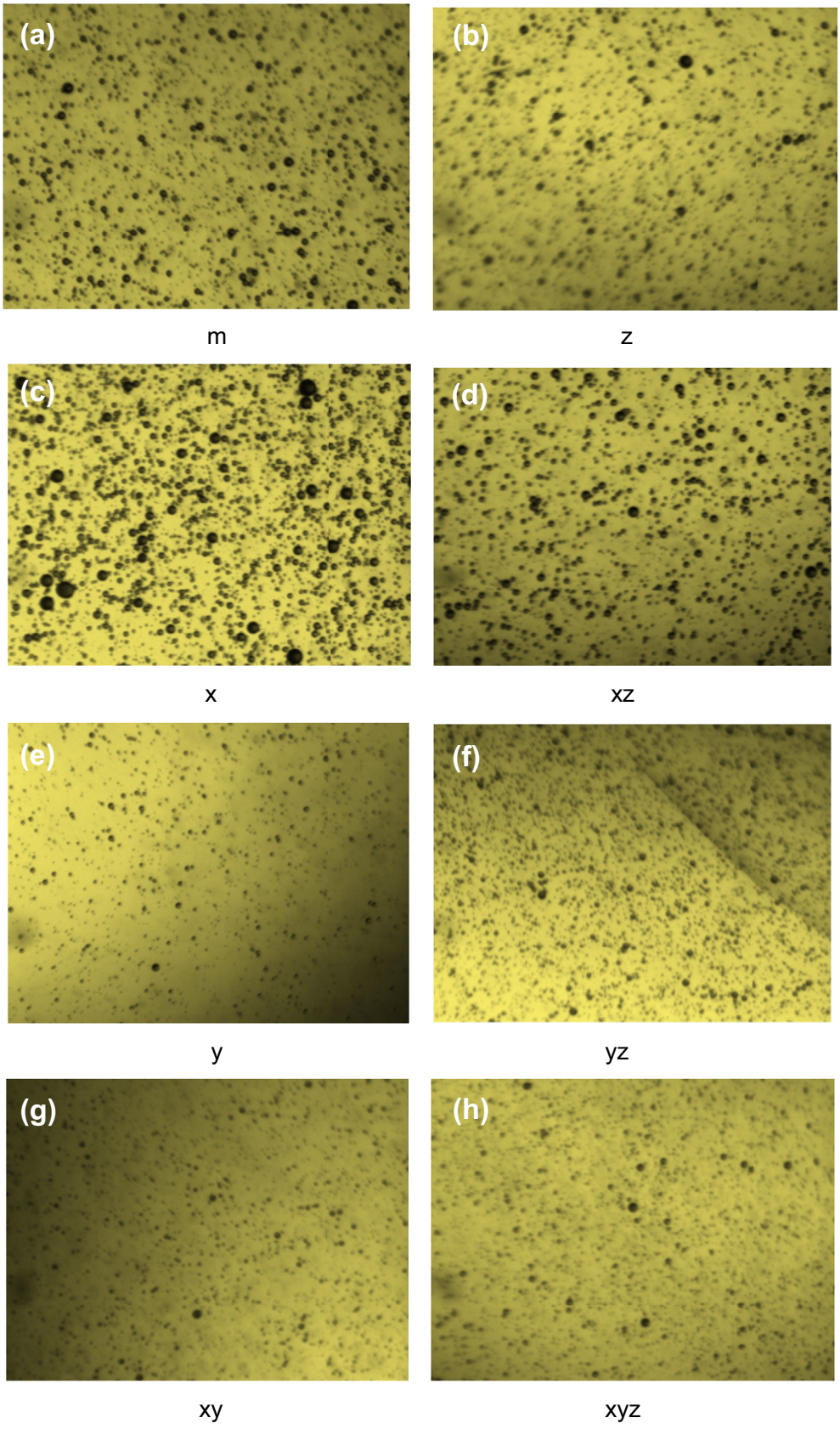

Figure 4. Images of Oil droplets under different pressures: (a) 1:32.5, energy dissipation rate $9.79*10^{-2}$, and 50 bar, (b) 1:32.5, energy dissipation rate $9.79*10^{-2}$ m^2/s^3, and 150 bar, (c) 1:17.5, energy dissipation rate $9.79*10^{-2}$ m^2/s^3, and 50 bar, and (d) 1:17.5, energy dissipation rate $9.79*10^{-2}$ m^2/s^3, and 150 bar, (e) 1:32.5, energy dissipation rate 3.23 m^2/s^3, and 50 bar, (f) 1:32.5, 3.23 m^2/s^3, and 150 bar, (g) 1:17.5, 3.23 m^2/s^3, and 50 bar, and (h) 1:17.5, 3.23 m^2/s^3, and 150 bar, respectively.

time. The major changes of the droplet sizes might be ascribed to the combination with each other or beak-up when they travel vertically through (e.g., resurfacing) the ocean. The stability could be the advantage of using chemical dispersants as a primary response tool to deal with oil spills in deep-water blow-out scenarios. The only exception occurred when mixing energy and DOR were set to 0.0979 m^2/s^3 and 1:32.5, respectively, meaning a lower dose of dispersant and a lower rate of dissipating energy, such that the effect of pressure may not be overwhelmed. Then the average droplet radius would change differently to 33.25 and 19.60 μm after being exposed to pressure at 50 and 150 bar, respectively. This observation suggested that, if the amounts of dispersant or mixing energy were insufficient, an application of dispersants at deep-water scenarios might result in relatively large oil droplets.

A decrease in DOR resulted in a relatively higher amount of dispersant in the same amount of oil, the interfacial tension of the resulting oil–dispersant mixture then decreased. Mukherjee et al. (2012) stated that an increase of DOR from 1:100 to 1:25 for Arabian light oil resulted in a decrease of interfacial tension from 210 to 180 N/m. Such a reduction in the oil-water interfacial tension was favored because of the easy breakage of oil sheen and thereby the formation of small droplets by lowering the energy required for creating new oil-water interfacial areas. In the present study, the average radius decreased from 33.25 to 25.14 μm when the DOR was changed from the low (1:32.5) to the high level (1:17.5), while shaking rate and pressure were set as 160 rpm and 50 bar, respectively (Table 1). However, when shaking rate was elevated to 240 rpm, the average radius was reduced from 21.95 to 19.81 μm, indicating that a higher shaking rate could compensate for the effect caused by DOR.

High shaking rate (240 rpm) could bring greater mixing energy (3.23 m^2/s^3) associated with lower Kolmogorov microscale (39.97μm) that could efficiently disperse oil into smaller droplet radius (19.81 μm), as compared to those (25.14 μm) at the low level (160 rpm; $9.79*10^{-2}$ m^2/s^3, 132.7μm for Kolmogorov microscale) when DOR and pressure were set as 1:17.5 and 50 bar, respectively. An increase of mixing energy provides additional energy to break large-sized oil droplets into smaller ones. Hence the droplet size distribution would be dominated by small droplets. Such a correlation among mixing energy, DOR, and the size of oil droplets had the same trend as experiments conducted under normal conditions (Li et al., 2011a, Yang et al., 2021). Mukherjee et al. (2012) reported an inverse dependency of oil droplet size on mixing energy during standard baffle tests. Additionally, the results fitted the changes of the droplet size of booming crude oil without dispersants from the impeller into an oil blowout high-pressure simulation system (Aman et al., 2015).

Meanwhile, the pressure loss did not significantly alter the droplet size of dispersed oil in all conditions (Fig. S1). The P value (>0.05) indicated that the probabilities of the insignificant difference between the two samples (difference = 0) were true for both 150 bar and 100 bar conditions.

The presented droplet size ranged from 8-124 μm, consistent with the range of ANS oil treated by Corexit 9500A generated by the subsurface oil injection system (0–100μm, DOR 1:20) (Conmy et al., 2017). Our results were compatible with the monitored droplet size of MC252 oil treated by Corexit 9500A using both laboratory and field tests (Li et al., 2009, 2011a; Lindo-Atichati et al., 2016b). Besides, Li et al. (2016) proposed a prediction method to estimate the droplet size distribution in deep water conditions, relying on d_{50}/D value (the medium value of droplets size/the diameter of the nozzle). The calculation results (0.007–0.016) from our medium size located at the range of observed d_{50}/D value (0.00–0.05). Additionally, the observed droplet size of pure South Louisiana sweet crude oil in a deep-sea blowout simulation system (150bar) (Malone et al., 2018).

3.3. Droplet radius regression using log-logistic distribution

Both log-normal and log-logistic distribution could fit droplet size of dispersed oil, as shown in Figure 5. Log-logistic regression was selected as a case to simulate the droplet size distribution. The histogram statistics and log-logistic regression of droplet radius are analyzed. Some histograms were illustrated in Figure 6 as examples. The log-logistic distribution well captured the characteristics of CDO under different experimental conditions. Such fitting can be further validated by the fact that the *p* values were all below 0.05 (Figure 7), implying that the droplet radius of CDO could be represented with statistical significance. The histograms also illustrated that when increasing energy dissipation rate from 0.0979 m^2/s^3 (Figure 5 (a)) to 3.23 m^2/s^3 (Figure 6 (b)), the radius of most oil droplets down-shifted from 15-45 to 15–25 μm. Contrastingly,

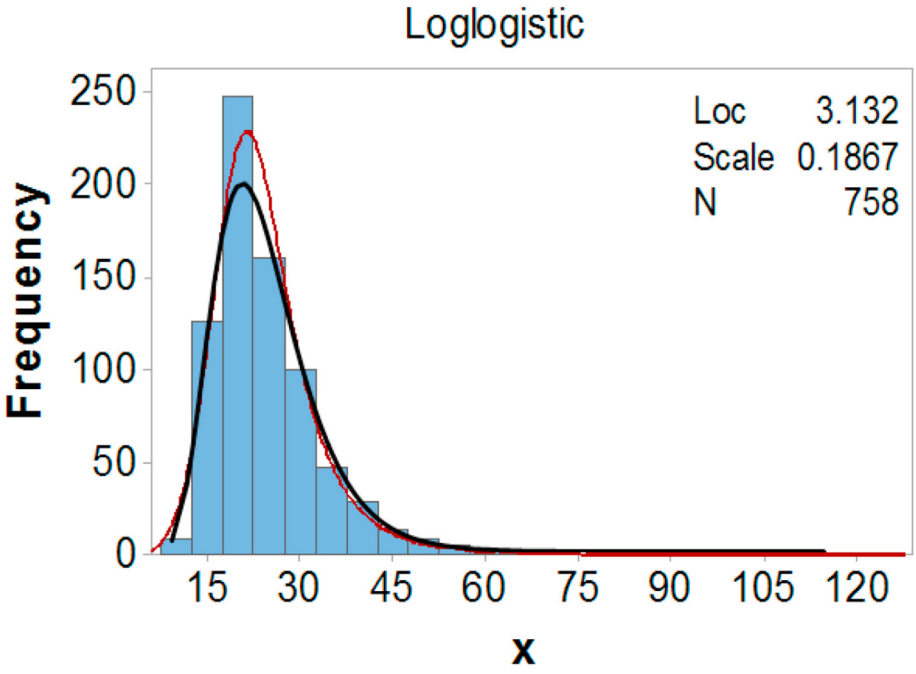

Figure 5. Log-logistic distribution and log-normal for simulation of droplet size distribution.

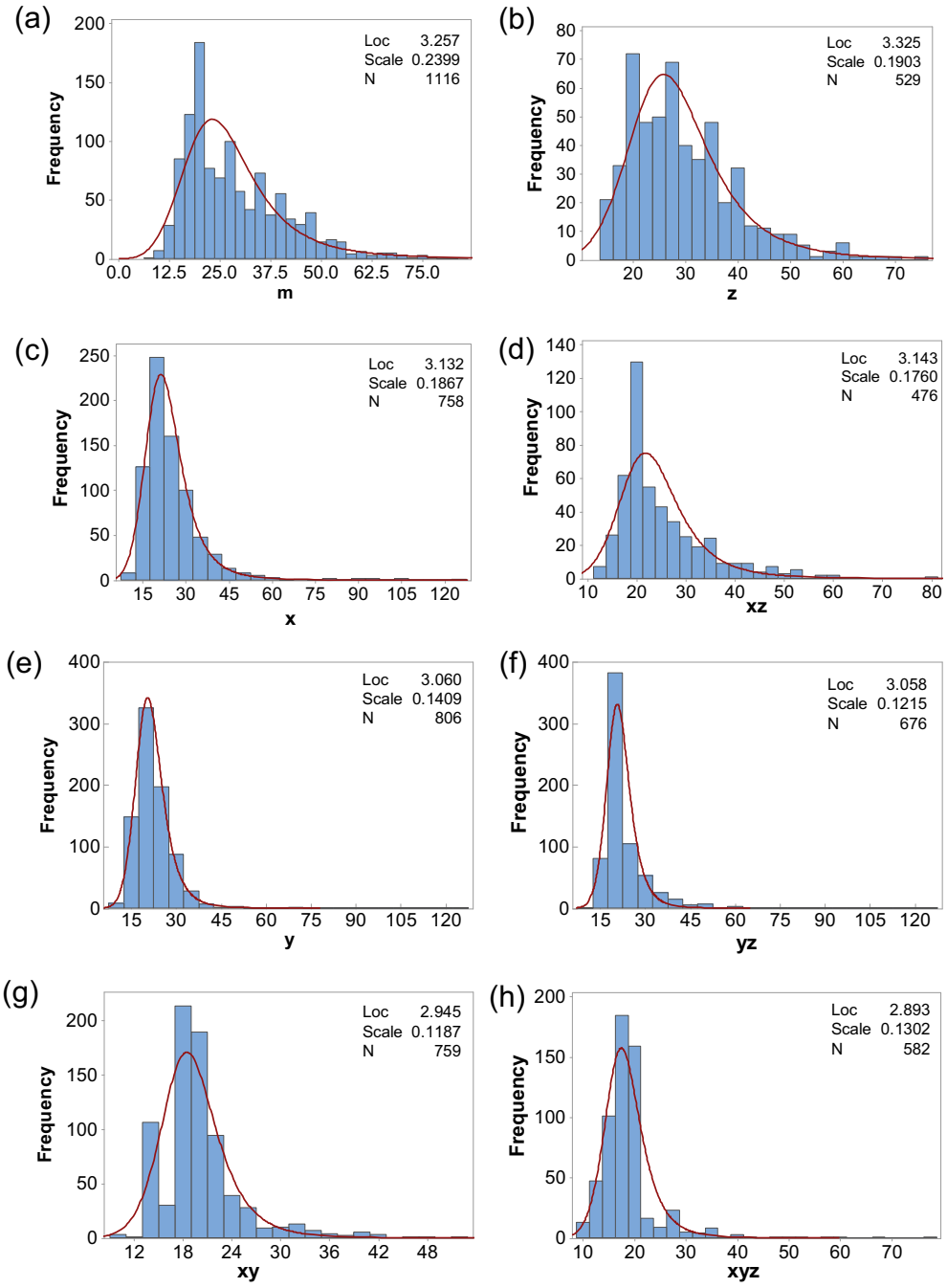

Figure 6. Histogram and log-logistic distribution regression for experimental runs when DOR, shaking rate and pressure was (a) 1:32.5, energy dissipation rate $9.79*10^{-2}$ m^2/s^3, and 50 bar, (b) 1:32.5, energy dissipation rate $9.79*10^{-2}$ m^2/s^3, and 150 bar, (c) 1:17.5, energy dissipation rate $9.79*10^{-2}$ m^2/s^3, and 50 bar, and (d) 1:17.5, energy dissipation rate $9.79*10^{-2}$ m^2/s^3, and 150 bar, (e) 1:32.5, energy dissipation rate 3.23 m^2/s^3, and 50 bar, (f) 1:32.5, energy dissipation rate 3.23 m^2/s^3, and 150 bar, (g) 1:17.5, energy dissipation rate 3.23 m^2/s^3, and 50 bar, and (h) 1:17.5, energy dissipation rate 3.23 m^2/s^3, and 150 bar, respectively.

increasing pressure from 50 (Figure 6 (c)) to 150 bar (Figure 6 (d)) did not show significant change on the distribution pattern.

The two shape parameters α (average) and β (variance) of log-logistic distribution were obtained for each of the eight experimental runs as shown in Table 2. They were further used as responses to study their relationships with DOR, mixing energy, and pressure via ANOVA. The results of ANOVA for α and β were summarized in Tables 5 and 6. The coded models for α and β were obtained as follows:

$$\alpha = 3.1 - 0.073 \times A - 0.11 \times B \tag{7}$$

$$\beta^{-1.45} = 11.3 + 4.6 \times B \tag{8}$$

The adjusted and predicted R^2 values were calculated as 0.96 and 0.93 for α, and 0.85 and 0.77 for β, respectively, indicating that both models had acceptable prediction accuracy. The effect of mixing energy was greater than that of DOR, which was in good agreement with Eqs. (5) and (6). The value of α appear red to be no correlation with pressure, but both negatively proportional to DOR and mixing energy. The relationships were close to those identified in Eq. (5) because α represents the average droplet radius after transformation. Remarkably, β was positively correlated with shaking rate only. The physical significance of β could be explained by the width of the distribution. The smaller the β, the narrower the distribution shape, which means that the size of most droplets would be close to the average. This trend indicated that a greater energy could result in more concentrated size distribution. Although the width of droplet size distribution varied with the pressure change in

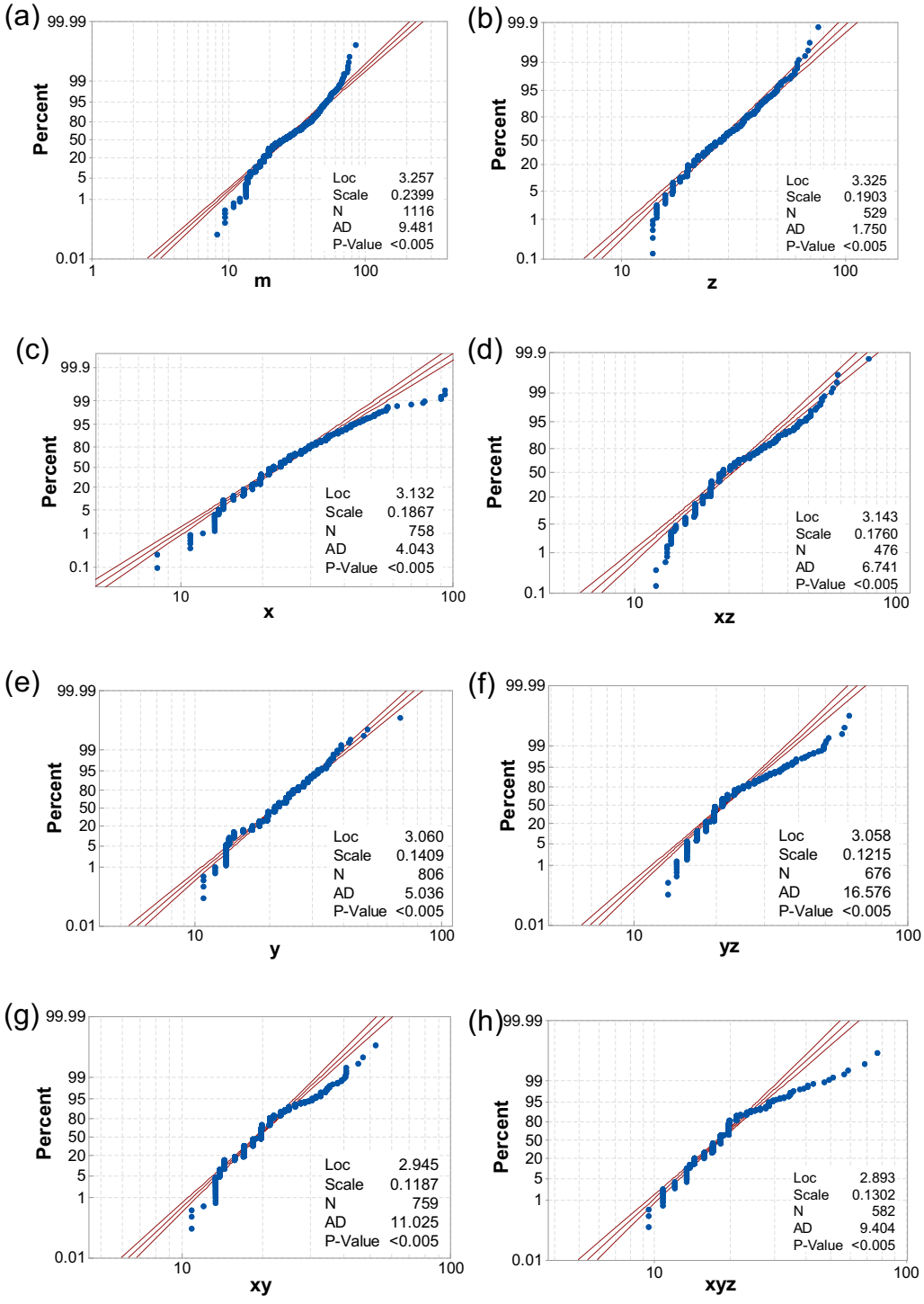

Figure 7. Probability plot of log-logistic distribution (95% confidence interval) for experimental runs when DOR, shaking rate and pressure was: (a) 1:32.5, energy dissipation rate $9.79*10^{-2}$ m^2/s^3, and 50 bar, (b) 1:32.5, energy dissipation rate $9.79*10^{-2}$ m^2/s^3, and 150 bar, (c) 1:17.5, energy dissipation rate $9.79*10^{-2}$ m^2/s^3, and 50 bar, and (d) 1:17.5, energy dissipation rate $9.79*10^{-2}$ m^2/s^3, and 150 bar, (e) 1:32.5, energy dissipation rate 3.23 m^2/s^3, and 50 bar, (f) 1:32.5, energy dissipation rate 3.23 m^2/s^3, and 150 bar, (g) 1:17.5, energy dissipation rate 3.23 m^2/s^3, and 50 bar, and (h) 1:17.5, energy dissipation rate 3.23 m^2/s^3, and 150 bar, respectively.

Table 5. ANOVA for the response of α

Source	Sum of squares	*df*	Mean square	*F*-value	*p*-value Prob > *F*	
Model	0.14	2	0.07	94.66	<0.0001	significant
A	0.04	1	0.04	56.41	0.0007	
B	0.10	1	0.10	132.90	<0.0001	
Residual	3.82×10^{-3}	5	7.64×10^{-4}			
Total	0.15	7				

Table 6. ANOVA for the transformed response of β

Source	Sum of squares	*df*	Mean square	*F*-value	*p*-value Prob > *F*	
Model	169.01	1	169.01	39.76	0.0007	significant
B	169.01	1	169.01	39.76	0.0007	
Residual	25.50	6	4.25			
Total	194.51	7				

Figure 6, The trend of the change of width is uncorrelated to the change of pressure. Additionally, as shown in Eqs. (7) and (8), the effect of pressure on the distribution of oil droplet size remains statistically insignificant. This finding verified that, when oil was well-mixed with dispersants, a pressure change may not cause any subsequent size change.

The distribution algorithms performed in this study implied highly reproducible and reasonable histogram functions for the prediction of droplet size distribution. The log-normal distribution was successfully fit the associated experimental observations under multiple circumstances, such as the with or without dispersants, the pure and CH4-saturated oil, as well as multiple types of oil, involving light oil (e.g., LSC, Macondo, and ANS) (Aman et al., 2015; Li et al., 2011a; Malone et al., 2018; Wang et al., 2016). Additionally, models regarding the behaviours of oil droplets, such as oil breakup and transport, were closely related to the distribution algorithms in this work (Hole et al., 2019; Johansen et al., 2013; Li et al., 2017).

The droplet distribution results could be used to predict or support the prediction of the behaviours of dispersed oil in the deep-water conditions, such as formation, breakup, vertical transport (buoyancy), coalescence, and biodegradation of oil droplets (Hole et al., 2019; Johansen et al., 2013; Li et al., 2017; North et al., 2015). The variations of the other factors (e.g., mixing energy and DOR) in this work also reflected the most common conditions when applying dispersants. The range of mixing energy (presented by shaking rate) could be transferred to the dissipate energy, which was needed for predicting oil transport and breakup behaviours. The findings had an important value by scientific evidence to better understand the dispersed oil behaviours under high pressure and potentially extend the existing results in shallow water to deep-water conditions.

4. Conclusions

This study investigated the influence of pressure on the size and distribution of chemically dispersed oil droplets after being exposed to multiple deep-water conditions. The effect of pressure coupled with oil-to-dispersant ratio (DOR), and mixing energy were examined through a two-level full factorial design. The experiments demonstrated that the size and distribution of oil droplets after dispersion were not significantly correlated with the change of pressure during most experimental runs. However, when DOR and mixing energy were both low, the average droplet radius would change differently to 33.25 and 19.60 μm at 50 and 150 bar, respectively, indicating that larger oil droplets may be formed as they resurface to the top of the ocean. High DOR may cause the interfacial tension of the oil-dispersant mixture to decrease and lead to easy breakage and formation of small droplets. A higher energy dissipation rate (lower Kolmogorov microscale) therefore break large-sized oil droplets into smaller ones. According to analysis of variance (ANOVA), no significant interaction between the three factors was identified. Both log-logistic distribution and log-normal distribution were applied for the regression of droplet size distribution with p values all below 0.05. The average, median, and distribution shape of chemically dispersed droplet size at different water depth could be predicted using the obtained ANOVA models. The research helped provide more scientific evidence to improve the understanding of dispersed oil behaviours under high pressure and support deep-sea oil spill research and potential extension of the existing results from shallow water to deep water conditions.

It is worth mentioning that this study faced some challenges, particularly due to the instrumental limitations. For example, the imaging constraint and the inherent deficiency of capturing droplets at multiple layers could affect the accuracy of droplet size/distribution observations; and the pressure increase by manual water injection brought small disturbance into the system. Besides, oil viscosity plays a vital role in the dispersion and formation of droplets. Higher viscosity refers to a larger cohesive force that can resist disruption and breakage of oil droplets into small ones. Viscosity was not included in this study, but it deserves more research effort in the future.

Declarations

Author contribution statement

Xing Song and Liang Jing: Conceived and designed the experiments; Performed the experiments; Analyzed and interpreted the data; Contributed reagents, materials, analysis tools or data; Wrote the paper.

Bing Chen and Baiyu Zhang: Conceived and designed the experiments; Contributed reagents, materials, analysis tools or data; Wrote the paper.

Zhiwen Zhu and Qinhong Cai: Conceived and designed the experiments; Performed the experiments; Analyzed and interpreted the data; Contributed reagents, materials, analysis tools or data.

Xudong Ye: Performed the experiments; Analyzed and interpreted the data; Wrote the paper.

Xiao Zheng: Performed the experiments; Analyzed and interpreted the data.

Stephen J. Hill: Performed the experiments; Contributed reagents, materials, analysis tools or data; Wrote the paper.

Funding statement

This work was supported by the Natural Sciences and Engineering Research Council of Canada, Canada (NSERC), Canada Foundation for Innovation (CFI), Government of Newfoundland and Labrador, Canada Ocean Science Center (OSC) of Memorial University, Canada.

Data availability statement

Data included in article/supplementary material/referenced in article.

Declaration of interests statement

The authors declare no conflict of interest.

Additional information

Supplementary content related to this article has been published online at https://doi.org/10.1016/j.heliyon.2021.e06291.

References

Abdelrahim, M., 2012. Measurement of interfacial tension in hydrocarbon/water/dispersant systems at deepwater conditions. Wiley Online Library.

Aman, Z.M., Paris, C.B., May, E.F., Johns, M.L., Lindo-Atichati, D., 2015. High-pressure visual experimental studies of oil-in-water dispersion droplet size. Chem. Eng. Sci. 127, 392–400.
Babinsky, E., Sojka, P., 2002. Modeling drop size distributions. Prog. Energy Combust. Sci. 28, 303–329.
Brandvik, P., Johansen, Ø., Farooq, U., Angell, G., Leirvik, F., 2014. Subsurface Oil Releases–Experimental Study of Droplet Distributions and Different Dispersant Injection Techniques Version 2. A Scaled Experimental Approach Using the SINTEF Tower basin. SINTEF Report.
Brandvik, P.J., Johansen, Ø., Leirvik, F., Farooq, U., Daling, P.S., 2013. Droplet breakup in subsurface oil releases–Part 1: experimental study of droplet breakup and effectiveness of dispersant injection. Mar. Pollut. Bull. 73, 319–326.
Camilli, R., Di Iorio, D., Bowen, A., Reddy, C.M., Techet, A.H., Yoerger, D.R., Whitcomb, L.L., Seewald, J.S., Sylva, S.P., Fenwick, J., 2011. Acoustic measurement of the Deepwater Horizon Macondo well flow rate. Proc. Natl. Acad. Sci. Unit. States Am.
Camilli, R., Reddy, C.M., Yoerger, D.R., Van Mooy, B.A., Jakuba, M.V., Kinsey, J.C., McIntyre, C.P., Sylva, S.P., Maloney, J.V., 2010. Tracking hydrocarbon plume transport and biodegradation at Deepwater Horizon. Science 330, 201–204.
Chen, F., Yapa, P.D., 2007. Estimating the oil droplet size distributions in deepwater oil spills. J. Hydraul. Eng. 133, 197–207.
Conmy, R., Robinson, B., King, T., Boufadel, M., Ryan, S., McIntyre, C., Abercrombie, M., Lee, K., 2017. Oil plume simulations: tracking oil droplet size distribution and fluorescence within high-pressure release jets. Int. Oil Spill Conf. Proc. 1230–1250.
Dippner, W., 2009. Mathematical modeling of the transport of pollution in water. Hydrol. Syst. Model 2, 204–246.
Gong, Y., Zhao, X., Cai, Z., O'reilly, S., Hao, X., Zhao, D., 2014. A review of oil, dispersed oil and sediment interactions in the aquatic environment: influence on the fate, transport and remediation of oil spills. Mar. Pollut. Bull. 79, 16–33.
Griggs, J.W., 2011. BP Gulf of Mexico oil spill. Energy LJ 32, 57.
Gros, J., Reddy, C.M., Nelson, R.K., Socolofsky, S.A., Arey, J.S., 2016. Simulating gas–liquid− water partitioning and fluid properties of petroleum under pressure: implications for deep-sea blowouts. Environ. Sci. Technol. 50, 7397–7408.
Hole, L.R., Dagestad, K.-F., Röhrs, J., Wettre, C., Kourafalou, V.H., Androulidakis, Y., Kang, H., Le Hénaff, M., Garcia-Pineda, O., 2019. The DeepWater Horizon oil slick: simulations of river front effects and oil droplet size distribution. J. Mar. Sci. Eng. 7, 329.
Johansen, Ø., 2003. Development and verification of deep-water blowout models. Mar. Pollut. Bull. 47, 360–368.
Johansen, Ø., Brandvik, P.J., Farooq, U., 2013. Droplet breakup in subsea oil releases–Part 2: predictions of droplet size distributions with and without injection of chemical dispersants. Mar. Pollut. Bull. 73, 327–335.
Kaku, V.J., Boufadel, M.C., Venosa, A.D., 2006. Evaluation of mixing energy in laboratory flasks used for dispersant effectiveness testing. J. Environ. Eng. 132, 93–101.
Khelifa, A., So, L., 2009. Effects of chemical dispersants on oil-brine interfacial tension and droplet formation, AMOP Technical Seminar on Environmental Contamination and Response. Ottawa (ON) 383–396.
Khelifa, A., Stoffyn-Egli, P., Hill, P.S., Lee, K., 2002. Characteristics of oil droplets stabilized by mineral particles: effects of oil type and temperature. Spill Sci. Technol. Bull. 8, 19–30.
Kujawinski, E.B., Kido Soule, M.C., Valentine, D.L., Boysen, A.K., Longnecker, K., Redmond, M.C., 2011. Fate of dispersants associated with the Deepwater Horizon oil spill. Environ. Sci. Technol. 45, 1298–1306.
Lemaire, B., Debier, C., Buc Calderon, P., Thomé, J.P., Stegeman, J., Mork, J., Rees, J.F.o, 2012. Precision-cut liver slices to investigate responsiveness of deep-sea fish to contaminants at high pressure. Environ. Sci. Technol. 46, 10310–10316.
Li, M., Garrett, C., 1998. The relationship between oil droplet size and upper ocean turbulence. Mar. Pollut. Bull. 36, 961–970.
Li, P., Weng, L., Niu, H., Robinson, B., King, T., Conmy, R., Lee, K., Liu, L., 2016. Reynolds number scaling to predict droplet size distribution in dispersed and undispersed subsurface oil releases. Mar. Pollut. Bull. 113, 332–342.
Li, Z., Lee, K., Kepkey, P.E., Mikkelsen, O., Pottsmith, C., 2011a. Monitoring dispersed oil droplet size distribution at the Gulf of Mexico Deepwater Horizon spill site. In: International Oil Spill Conference Proceedings (IOSC). American Petroleum Institute, p. abs377.
Li, Z., Lee, K., King, T., Boufadel, M.C., Venosa, A.D., 2009. Evaluating chemical dispersant efficacy in an experimental wave tank: 2—significant factors determining in situ oil droplet size distribution. Environ. Eng. Sci. 26, 1407–1418.
Li, Z., Lee, K., King, T., Niu, H., Boufadel, M.C., Venosa, A.D., 2011b. Application of entropy analysis of in situ droplet-size spectra in evaluation of oil chemical dispersion efficacy. Mar. Pollut. Bull. 62, 2129–2136.
Li, Z., Spaulding, M., McCay, D.F., Crowley, D., Payne, J.R., 2017. Development of a unified oil droplet size distribution model with application to surface breaking waves and subsea blowout releases considering dispersant effects. Mar. Pollut. Bull. 114, 247–257.
Lindo-Atichati, D., Paris, C., Le Hénaff, M., Schedler, M., Juárez, A.V., Müller, R., 2016a. Simulating the effects of droplet size, high-pressure biodegradation, and variable flow rate on the subsea evolution of deep plumes from the Macondo blowout. Deep Sea Res. Part II Top. Stud. Oceanogr. 129, 301–310.
Lindo-Atichati, D., Paris, C.B., Le Hénaff, M., Schedler, M., Juárez, A.V., Müller, R., 2016b. Simulating the effects of droplet size, high-pressure biodegradation, and variable flow rate on the subsea evolution of deep plumes from the Macondo blowout. Deep Sea Res. Part II Top. Stud. Oceanogr. 129, 301–310.
Malone, K., Pesch, S., Schlüter, M., Krause, D., 2018. Oil droplet size distributions in deep-sea blowouts: influence of pressure and dissolved gases. Environ. Sci. Technol. 52, 6326–6333.
Mukherjee, B., Wrenn, B.A., Ramachandran, P., 2012. Relationship between size of oil droplet generated during chemical dispersion of crude oil and energy dissipation rate: dimensionless, scaling, and experimental analysis. Chem. Eng. Sci. 68 (1), 432–442.
North, E.W., Adams, E.E., Thessen, A.E., Schlag, Z., He, R., Socolofsky, S.A., Masutani, S.M., Peckham, S.D., 2015. The influence of droplet size and biodegradation on the transport of subsurface oil droplets during the Deepwater Horizon spill: a model sensitivity study. Environ. Res. Lett. 10, 24016.
Pradillon, F., Shillito, B., Chervin, J.-C., Hamel, G., Gaill, F., 2004. Pressure vessels for in vivo studies of deep-sea fauna. High Pres. Res. 24, 237–246.
Prince, R.C., Nash, G.W., Hill, S.J., 2016. The biodegradation of crude oil in the deep ocean. Mar. Pollut. Bull. 111, 354–357.
Ryerson, T.B., Camilli, R., Kessler, J.D., Kujawinski, E.B., Reddy, C.M., Valentine, D.L., Atlas, E., Blake, D.R., De Gouw, J., Meinardi, S., 2012. Chemical data quantify Deepwater Horizon hydrocarbon flow rate and environmental distribution. Proc. Natl. Acad. Sci. Unit. States Am. 109, 20246–20253.
Scheibye, K., Christensen, J.H., Johnsen, A.R., 2017. Biodegradation of crude oil in Arctic subsurface water from the Disko Bay (Greenland) is limited. Environ. Pollut. 223, 73–80.
Socolofsky, S.A., 2001. Laboratory experiments of multi-phase plumes in stratification and crossflow. Massachusetts Institute of Technology.
Socolofsky, S.A., Adams, E.E., Sherwood, C.R., 2011. Formation dynamics of subsurface hydrocarbon intrusions following the Deepwater Horizon blowout. Geophys. Res. Lett. 38.
Spier, C., Stringfellow, W.T., Hazen, T.C., Conrad, M., 2013. Distribution of hydrocarbons released during the 2010 MC252 oil spill in deep offshore waters. Environ. Pollut. 173, 224–230.
Turner, R.E., Rabalais, N.N., Overton, E.B., Meyer, B.M., McClenachan, G., Swenson, E.M., Besonen, M., Parsons, M.L., Zingre, J., 2019. Oiling of the continental shelf and coastal marshes over eight years after the 2010 Deepwater Horizon oil spill. Environ. Pollut. 252, 1367–1376.
van der Tuuk Opedal, N., Sørland, G., Sjöblom, J., 2009. Methods for droplet size distribution determination of water-in-oil emulsions using low-field NMR. Diff. Fund. 7, 1–29.
Venosa, A., Holder, E., 2007. Biodegradability of dispersed crude oil at two different temperatures. Mar. Pollut. Bull. 54, 545–553.
Venosa, A.D., King, D.W., Sorial, G.A., 2002. The baffled flask test for dispersant effectiveness: a round robin evaluation of reproducibility and repeatability. Spill Sci. Technol. Bull. 7, 299–308.
Vilcáez, J., Li, L., Hubbard, S.S., 2013. A new model for the biodegradation kinetics of oil droplets: application to the Deepwater Horizon oil spill in the Gulf of Mexico. Geochem. Trans. 14, 4.
Wang, Z., DiMarco, S.F., Socolofsky, S.A., 2016. Turbulence measurements in the northern Gulf of Mexico: application to the Deepwater Horizon oil spill on droplet dynamics. Deep Sea Res. Oceanogr. Res. Pap. 109, 40–50.
Yang, M., Chen, B., Xin, X., Song, X., Liu, J., Dong, G., Lee, K., Zhang, B., 2021. Interactions between microplastics and oil dispersion in the marine environment. J. Hazard. Mater. 403, 123944.
Zhang, K., Zhang, B., Song, X., Liu, B., Jing, L., Chen, B., 2018. Generation of shrimp waste-based dispersant for oil spill response. Environ. Sci. Pollut. Res. 25 (10), 9443–9453.
Zhao, L., Boufadel, M.C., King, T., Robinson, B., Gao, F., Socolofsky, S.A., Lee, K., 2017. Droplet and bubble formation of combined oil and gas releases in subsea blowouts. Mar. Pollut. Bull. 120, 203–216.
Zhao, L., Boufadel, M.C., Socolofsky, S.A., Adams, E., King, T., Lee, K., 2014a. Evolution of droplets in subsea oil and gas blowouts: Development and validation of the numerical model VDROP-J. Mar. Pollut. Bull. 83, 58–69.
Zhao, L., Shaffer, F., Robinson, B., King, T., D'Ambrose, C., Pan, Z., Gao, F., Miller, R.S., Conmy, R.N., Boufadel, M.C., 2016a. Underwater oil jet: hydrodynamics and droplet size distribution. Chem. Eng. J. 299, 292–303.
Zhao, L., Torlapati, J., Boufadel, M.C., King, T., Robinson, B., Lee, K., 2014b. VDROP: a comprehensive model for droplet formation of oils and gases in liquids-Incorporation of the interfacial tension and droplet viscosity. Chem. Eng. J. 253, 93–106.
Zhao, L., Wang, B., Armenante, P.M., Conmy, R., Boufadel, M.C., 2016b. Characterization of turbulent properties in the EPA baffled flask for dispersion effectiveness testing. J. Environ. Eng. 142, 04015044.